NASA TECHNICAL NOTE

NASA TN D-7461

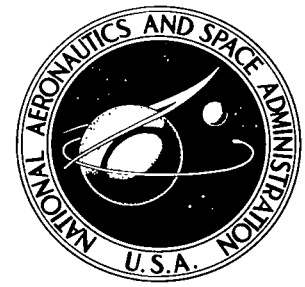

NASA TN D-7461

FLIGHT CALIBRATION TESTS OF A NOSE-BOOM-MOUNTED FIXED HEMISPHERICAL FLOW-DIRECTION SENSOR

by Katharine H. Armistead and Lannie D. Webb

Flight Research Center
Edwards, Calif. 93523

NATIONAL AERONAUTICS AND SPACE ADMINISTRATION • WASHINGTON, D. C. • OCTOBER 1973

1. Report No.	2. Government Accession No.	
NASA TN D-7461		

4. Title and Subtitle

FLIGHT CALIBRATION TESTS OF A NOSE-BOOM-MOUNTED FIXED HEMISPHERICAL FLOW-DIRECTION SENSOR

5. Report Date: October 1973

6. Performing Organization Code:

7. Author(s)

Katharine H. Armistead and Lannie D. Webb

8. Performing Organization Report No.: H-779

9. Performing Organization Name and Address

NASA Flight Research Center
P. O. Box 273
Edwards, California 93523

10. Work Unit No.: 501-38-16-00

11. Contract or Grant No.:

12. Sponsoring Agency Name and Address

National Aeronautics and Space Administration
Washington, D. C. 20546

13. Type of Report and Period Covered: Technical Note

14. Sponsoring Agency Code:

15. Supplementary Notes

16. Abstract

Flight calibrations of a fixed hemispherical flow angle-of-attack and angle-of-sideslip sensor were made from Mach numbers of 0.5 to 1.8. Maneuvers were performed by an F-104 airplane at selected altitudes to compare the measurement of flow angle of attack from the fixed hemispherical sensor with that from a standard angle-of-attack vane.

The hemispherical flow-direction sensor measured differential pressure at two angle-of-attack ports and two angle-of-sideslip ports in diametrically opposed positions. Stagnation pressure was measured at a center port. The results of these tests showed that the calibration curves for the hemispherical flow-direction sensor were linear for angles of attack up to 13°. The overall uncertainty in determining angle of attack from these curves was ±0.35° or less.

A Mach number position error calibration curve was also obtained for the hemispherical flow-direction sensor. The hemispherical flow-direction sensor exhibited a much larger position error than a standard uncompensated pitot-static probe.

17. Key Words (Suggested by Author(s))

Flow-direction sensor
Hemispherical flow-direction sensor
Angle-of-attack measurements

18. Distribution Statement

Unclassified - Unlimited

19. Security Classif. (of this report)	20. Security Classif. (of this page)	21. No. of Pages	22. Price*
Unclassified	Unclassified	27	Domestic, $3.00 Foreign, $5.50

* For sale by the National Technical Information Service, Springfield, Virginia 22151

FLIGHT CALIBRATION TESTS OF A NOSE-BOOM-MOUNTED FIXED HEMISPHERICAL FLOW-DIRECTION SENSOR

Katharine H. Armistead and Lannie D. Webb
Flight Research Center

INTRODUCTION

The accurate measurement of angle of attack and angle of sideslip is of prime importance for the analysis of flight-test data. At the NASA Flight Research Center, the vane type of flow-direction sensor has been used in most flight research programs, but increasing aircraft performance capabilities have exposed the vanes to higher temperatures which have occasionally caused structural damage. As a consequence, another type of flow-direction sensor would be desirable for high-performance aircraft. Thus a hemispherical flow-direction sensor, which has more structural rigidity than a vane type of sensor, was flight tested on an F-104 airplane (fig. 1). This probe makes use of differential pressure measurements to determine flow direction.

Hemispherical flow-direction sensors have been tested extensively in wind tunnels (refs. 1 to 4). During these tests the probes were mounted on a sting and exposed to a uniform free-stream flow. In the F-104 tests a hemispherical flow-direction sensor was strut-mounted on the aircraft's nose boom close to an angle-of-attack vane and an angle-of-sideslip vane.

This report presents comparisons of the angle-of-attack measurements made by the F-104's flow-direction sensor and the angle-of-attack vane. In addition, the hemispherical flow-direction sensor's calibration is compared with wind-tunnel data to determine whether there was any interference from the vanes or the nose boom. Finally, the report evaluates the usefulness of the sensor as an aircraft airspeed sensor.

SYMBOLS

Physical quantities in this report are given in the International System of Units (SI) and parenthetically in U.S. Customary Units. The measurements were made in U.S. Customary Units. Factors relating the two systems are presented in reference 5.

h	geometric altitude, km (ft)
M	Mach number
M_i	indicated Mach number
M_∞	true Mach number
p_t	stagnation pressure measured by the pitot-static probe, kN/m^2 (lb/ft^2)
p_{t_5}	stagnation pressure measured by the hemispherical flow-direction sensor, kN/m^2 (lb/ft^2)
p_1, p_3	angle-of-attack pressures measured by the hemispherical flow-direction sensor, kN/m^2 (lb/ft^2)
p_2, p_4	angle-of-sideslip pressures measured by the hemispherical flow-direction sensor, kN/m^2 (lb/ft^2)
p_∞	ambient pressure, kN/m^2 (lb/ft^2)
q	free-stream dynamic pressure, kN/m^2 (lb/ft^2)
q_c	differential pressure for the pitot-static probe, $p_t - p_\infty$, kN/m^2 (lb/ft^2)
q_{c_5}	differential pressure for the hemispherical flow-direction sensor, $p_{t_5} - \frac{p_2 + p_4}{2}$, kN/m^2 (lb/ft^2)
α	angle of attack, deg
β	angle of sideslip, deg
Δp_α	differential pressure between the two angle-of-attack ports, $p_3 - p_1$, kN/m^2 (lb/ft^2)
Δp_β	differential pressure between the two angle-of-sideslip ports, $p_4 - p_2$, kN/m^2 (lb/ft^2)

DESCRIPTION OF APPARATUS

Flow-Direction Sensor

A flow-direction sensor with five pressure orifices was fabricated at the NASA Flight Research Center and attached by a special support to the nose boom of an F-104 airplane (figs. 2 and 3). The support for the sensor and the sensor itself were aluminum, and they were precisely alined with the airplane's centerline. The sensor had a diameter of 1.90 centimeters (0.75 inch) with 0.31-centimeter-(0.12-inch-) diameter pressure orifices. One port was centrally located, and the other four were 45° from the center port in orthogonal planes (figs. 4(a) to 4(c)). The difference in pressure between ports 1 and 3 was used for the measurement of angle of attack, and the difference in pressure between ports 2 and 4 was used for the measurement of angle of sideslip. The fifth orifice was used to measure local stagnation pressure. The tip of the hemispherical flow-direction sensor was opposite the angle-of-attack vane (ref. 6), and each was equidistant from the nose-boom centerline and the tip of the nose boom.

Variable-capacitance pressure transducers in the airplane's nose cone as close to the nose boom as possible were used to measure pressures from the flow-direction sensor. Each cell used to measure angle-of-attack and angle-of-sideslip pressures had a range of 0 to 105 kN/m^2 (0 to 2200 lb/ft^2), and the cell used to measure stagnation pressure had a range of 0 to 144 kN/m^2 (0 to 3000 lb/ft^2).

Pitot-Static Probe

The pitot-static probe used in the tests was a standard NACA model A-6 probe (ref. 6) except that the total temperature element was replaced by the fixed flow-direction sensor. The pitot-static probe sensed static and stagnation pressures for the determination of airspeed and pressure altitude. The installation also included the free-floating angle-of-attack and angle-of-sideslip vanes (fig. 2). Both the angle-of-attack and angle-of-sideslip measurements were sensed by a synchro transmitter mounted on the angle-of-attack and angle-of-sideslip vane shafts. The pitot-static probe's pressure-sensing system consisted of two precision pressure transducers. The airspeed sensor was a differential cell with a range of 0 to 249 kN/m^2 (0 to 5200 lb/ft^2), and the altitude sensor was an absolute cell with a range of 0 to 101 kN/m^2 (0 to 2100 lb/ft^2).

DATA RECORDING

The analog output from the pressure transducers was encoded by a pulse code modulation system (PCM). The binary code output of the PCM system was transmitted to a ground station and was also recorded onboard the aircraft. These data were processed by a ground-based computer, which provided corrected pressure data in engineering units.

FLIGHT-TEST PROCEDURE

Before the flight data were compared with wind-tunnel data, an airspeed calibration was made. Ground radars were used to track the F-104 airplane as it performed level accelerations and decelerations. The airplane's position error was determined by correlating the airplane altitude determined by the radars with the ambient pressure sensed by a rawinsonde balloon (ref. 7).

To obtain flight data from the hemispherical flow-direction sensor the following procedures were followed. The airplane performed pushovers and pullups at selected Mach numbers and at fixed altitudes of 7.6 kilometers (25,000 feet), 10.7 kilometers (35,000 feet), and 12.2 kilometers (40,000 feet). It also flew at constant angles of attack in 2° increments at the selected test conditions. Except for the pullups and pushovers, the airplane was flown in the clean configuration and near 1g conditions. The pilot maintained quasi-steady test conditions for a while before data were taken to stabilize the pressure measurements. Flight data were obtained over an angle-of-attack range of 0° to 13°, an angle-of-sideslip range of $\pm 3^\circ$, and a Mach number range of 0.5 to 1.8. Most of the flight data were obtained at an angle of sideslip near 0° to make it easier to correlate the wind-tunnel and flight data.

ACCURACY

An error analysis of the precision transducers of the pitot-static probe was made by analyzing data from laboratory tests, hangar calibration checks, and pre- and postflight zeros. The analysis indicated that the measurement of ambient pressure was accurate to ± 0.143 kN/m^2 (± 3.0 lb/ft^2) on the ground. Over the altitude range of interest (6.1 km (20,000 ft) to 12.2 km (40,000 ft)) the measurement of pitot-static probe differential pressure had an accuracy of ± 0.383 kN/m^2 (± 8.0 lb/ft^2).

The error in the stagnation pressure measurement is a function of the combined inaccuracy of the airspeed and the static pressure measurements. The root-sum-square error in the stagnation pressure measurement was therefore approximately ± 0.409 kN/m^2 (± 8.5 lb/ft^2).

The static pressure error of ± 0.143 kN/m^2 (± 3.0 lb/ft^2) and the stagnation pressure error of ± 0.409 kN/m^2 (± 8.5 lb/ft^2) were used for the Mach number error analysis. Mach number uncertainty due to instrument error was calculated by root-sum-square analysis, and the resulting errors are shown in table 1.

The accuracy of the variable-capacitance pressure cells used to measure pressures in the fixed flow-direction sensor was determined from laboratory tests. The

accuracy of the cells was as follows:

Δp_α . . .	± 0.383 kN/m^2 (± 8.0 lb/ft^2)
Δp_β . . .	± 0.316 kN/m^2 (± 6.6 lb/ft^2)
p_{t_5} . . .	± 0.143 kN/m^2 (± 3.0 lb/ft^2)
p_1 . . .	± 0.095 kN/m^2 (± 2.0 lb/ft^2)

The angle-of-attack and angle-of-sideslip vanes, which were used to correlate flow-direction readings with pressures measured by the hemispherical flow-direction sensor, had an uncertainty of $\pm 0.25^\circ$. This excludes such uncertainties as flow field upwash and boom bending.

RESULTS AND DISCUSSION

Comparison of Sensitivity Parameters

The flight data that minimized pressure lag were selected for analysis. For this reason the flight data analyzed were for a rate of change of altitude of less than ± 23 m/sec (± 75 ft/sec). The flight data selected for comparison with wind-tunnel data were for angles of sideslip of less than $\pm 0.5^\circ$.

Sensitivity parameter $\Delta\left(\frac{\Delta p_\alpha}{q_c}\right)\frac{1}{\Delta\alpha}$. – Figures 5(a) to 5(d) present the ratio $\frac{\Delta p_\alpha}{p_\infty}$ as a function of angle of attack for Mach numbers from 0.5 to 1.8. The fairings of the data points were linear for angles of attack up to 13°. The data scatter is within the estimated uncertainty of ± 0.01 to ± 0.18 for a given Mach number and angle of attack for the altitude range from 6.1 kilometers (20,000 feet) to 12.2 kilometers (40,000 feet). The effects of altitude are also within the data scatter, indicating that altitude had little if any effect on the data. The data shown in figure 5 were used to determine the sensitivity of the hemispherical flow-direction sensor to changes in Mach number. To allow the flight data to be compared directly with the wind-tunnel data from reference 4, the slope $\Delta\left(\frac{\Delta p_\alpha}{p_\infty}\right)\frac{1}{\Delta\alpha}$ was changed to $\Delta\left(\frac{\Delta p_\alpha}{q_c}\right)\frac{1}{\Delta\alpha}$ by multiplying it by $\left(\frac{q_c}{p_\infty}\right)^{-1}$ for each Mach number in figure 5. Data from the

other wind-tunnel tests (refs. 1 to 3) were also used to calculate $\Delta\left(\frac{\Delta p_\alpha}{q_c}\right)\frac{1}{\Delta\alpha}$ and compared with the flight-determined sensitivity parameter.

Figure 6 shows a plot of $\Delta\left(\frac{\Delta p_\alpha}{q_c}\right)\frac{1}{\Delta\alpha}$ as a function of Mach number as determined from flight data and the wind-tunnel tests (refs. 1 to 4). The data in references 1 and 2 are for supersonic Mach numbers only and were obtained from a hemispherical flow-direction sensor mounted directly on a sting with no afterbody. Reference 4 presents subsonic, transonic, and supersonic data for an isolated probe. The data in reference 3 were for a hemispherical flow-direction sensor which had a fairing behind the probe for part of the test runs.

The subsonic flight data are in fairly good agreement with the wind-tunnel data from references 3 and 4. Below Mach 0.8, the flight data agree more closely with the wind-tunnel data from reference 3 than with the data from reference 4. The agreement between the flight data and the wind-tunnel data from references 3 and 4 improves near $M = 1.0$. The agreement between the flight and the wind-tunnel data is good for Mach numbers from 1.2 to 1.8 (refs. 1, 2, and 4).

Figure 6 can be used to define a calibration curve for use by an air-data computer to obtain angle of attack from the pressure measurements. A curve fit and an equation were obtained for the flight data in figure 6. An equation for the calibration curve of angle of attack takes the form

$$\alpha = \frac{\Delta p_\alpha}{q_c}\left(a_0 + a_1 M_\infty + a_2 M_\infty^2 + \ldots + a_n M_\infty^n\right) \qquad (1)$$

where

$a_0 = 0.15657$ $\qquad$ $a_3 = 0.10768$

$a_1 = -0.12876$ $\qquad$ $a_4 = -0.04719$

$a_2 = -0.04514$ $\qquad$ $a_5 = 0.00660$

Average angle-of-attack errors were calculated by using six terms in equation (1) and the errors in the measured pressure quantities. (See ACCURACY.) The resulting errors are listed in table 2.

Since the pressure measurements for the angle-of-attack determination were compared with the measurements from the angle-of-attack vane, a root-sum-square calculation was made by using values from table 2 and an uncertainty of $\pm 0.25^\circ$ for the vane measurements. The values from table 2 and the results of the calculations are presented in figure 7. As shown in figure 7, the uncertainty in the angle-of-attack determination decreases with increasing dynamic pressure. For example, above a dynamic pressure of approximately 40 kN/m^2 (835 lb/ft^2), the average uncertainty for the combined errors is less than approximately $\pm 0.30^\circ$. For the dynamic

pressure range above 30 kN/m^2 (626 lb/ft^2), the average angle-of-attack uncertainty is less than $\pm 0.35^\circ$.

Sensitivity parameter $\Delta\left(\frac{\Delta p_\alpha}{p_t}\right)\frac{1}{\Delta\alpha}$. – Figure 8 presents the sensitivity parameter $\Delta\left(\frac{\Delta p_\alpha}{p_t}\right)\frac{1}{\Delta\alpha}$ for the hemispherical flow-direction sensor as a function of Mach number. The flight data are the data presented in figure 5 calculated in terms of $\Delta\left(\frac{\Delta p_\alpha}{p_t}\right)\frac{1}{\Delta\alpha}$. One of the curves is a fairing of the wind-tunnel data presented in figure 6 from references 1 to 4. The other curve is data from reference 8 for a similar hemispherical flow-direction sensor with only four orifices that was mounted next to a pitot-static probe.

The flight data are below the two faired wind-tunnel curves for Mach numbers of 0.5 and 0.6 and agree with the wind-tunnel data for Mach numbers from 0.7 to 0.9. The flight data for the transonic Mach numbers dip below the wind-tunnel data from references 1 to 4. A similar dip occurs above Mach 1.0 in the wind-tunnel data from reference 8. Interference from the supporting structures of the hemispherical flow-direction sensor and the pitot-static probe may have caused this deviation from the wind-tunnel data from references 1 to 4, which were for isolated probes. The dip in the flight data may be larger than the dip in the wind-tunnel data from reference 8 because in the flight data there was interference from the angle-of-attack vane as well as from the hemispherical flow-direction sensor and the pitot-static probe.

The wind-tunnel data agree well with the flight data for Mach numbers from 1.2 to 1.7, so it may be concluded that interference from the supporting strut and the pitot-static probe in this Mach number range was negligible. Above Mach 1.7, the wind-tunnel data for the fixed-direction sensor and pitot-static probe combination (ref. 8) diverge somewhat from the wind-tunnel data where no pitot-static probe was present (refs. 1 to 4).

Sensitivity parameter $\Delta\left(\frac{\Delta p_\alpha}{q_{c_5}}\right)\frac{1}{\Delta\alpha}$. – Figure 9(a) shows a comparison of flight data with wind-tunnel data from reference 4 in terms of the sensitivity parameter $\Delta\left(\frac{\Delta p_\alpha}{q_{c_5}}\right)\frac{1}{\Delta\alpha}$. The flight data vary from a maximum value of approximately 0.08 at a Mach number of 0.6 to approximately 0.07 at $M \approx 1.8$. The wind-tunnel data that are available show a larger variation than the flight data. The wind-tunnel data range from approximately 0.09 at Mach 0.6 to approximately 0.08 at Mach 0.8.

Figure 9(b) shows a plot of the two sensitivity parameters $\Delta\left(\frac{\Delta p_\alpha}{q_c}\right)\frac{1}{\Delta\alpha}$ and $\Delta\left(\frac{\Delta p_\alpha}{q_{c_5}}\right)\frac{1}{\Delta\alpha}$ as a function of Mach number. The parameter $\Delta\left(\frac{\Delta p_\alpha}{q_c}\right)\frac{1}{\Delta\alpha}$ was obtained from equation (1) by taking the average of all the flight and wind-tunnel data in figure 6. The two parameters differ significantly. The difference is the result of using different pressure values to calculate q_c and q_{c_5}. For q_c, ambient pressure was subtracted from p_t, whereas for q_{c_5} $\frac{p_2 + p_4}{2}$ was subtracted from p_{t_5}. Figure 9(b) shows that the parameter $\Delta\left(\frac{\Delta p_\alpha}{q_{c_5}}\right)\frac{1}{\Delta\alpha}$ is linear and that it is not very sensitive to Mach number, which is advantageous. In addition, $\Delta\left(\frac{\Delta p_\alpha}{q_{c_5}}\right)\frac{1}{\Delta\alpha}$ is larger than $\Delta\left(\frac{\Delta p_\alpha}{q_c}\right)\frac{1}{\Delta\alpha}$, which reduces the percentage of uncertainty and allows angle of attack to be calculated with greater accuracy.

Comparison of Stagnation Pressures

Figure 10 compares stagnation pressures p_t and p_{t_5} in terms of the ratio $\frac{p_t - p_{t_5}}{p_t}$ as a function of Mach number. Over most of the Mach number range, the differences between the stagnation pressures sensed by the pitot-static probe and the hemispherical flow-direction sensor are within the accuracy of the measurements. The subsonic data cover an angle-of-attack range from 0° to 13°, and the supersonic data cover an angle-of-attack range from 2° to 7°. From Mach 0.5 to 1.6, the ratio $\frac{p_t - p_{t_5}}{p_t}$ never exceeds approximately ±0.025. The data then become more negative, reaching a value of -0.050 at $M \approx 1.9$.

It may be concluded from figure 10 that up to a Mach number of 1.6 the pitot-static probe and the hemispherical flow-direction sensor did not influence one another's stagnation pressure measurements, nor did the strut and support have any detectable effect on the stagnation pressure measurements.

Comparison of Mach Number Errors

Figure 11 shows a Mach number position error curve obtained from typical data in reference 9 for an A-6 NACA pitot-static probe installed on a nose boom. Also shown in figure 11 is the Mach number position error derived from the hemispherical flow-direction sensor. The data points for the hemispherical flow-direction sensor

were calculated using p_{t_5} for stagnation pressure and $\frac{p_2 + p_4}{2}$, $\frac{p_1 + p_3}{2}$, or $\frac{p_1 + p_2 + p_3 + p_4}{4}$ for probe static pressure in the Rayleigh pitot equation (ref. 10). Use of any of the three probe static pressures in conjunction with p_{t_5} results in approximately the same curve as that shown in figure 11 because the angles of attack were less than 7° for the supersonic speeds. Figure 11 shows that the hemispherical flow-direction sensor has a much larger position error than the pitot-static probe and that the error increases linearly with Mach number.

Also shown is a data point from the static ports on the cylindrical portion of a hemispherical flow-direction sensor (ref. 2) for a Mach number of 1.4. Taking Mach 1.4 as the point of comparison, the following Mach number errors were found:

Static port surface	Position error
Cylindrical –	
Pitot-static probe	0.007
Hemispherical flow-direction sensor (ref. 2)	-0.060
Hemispherical –	
Hemispherical flow-direction sensor (45° from the center port)	0.650

The Mach number position error obtained with the hemispherical flow-direction sensor by using static ports 45° from the center port is nearly linear and approximately an order of magnitude larger than the error for the static ports on the cylindrical surface at right angles to the flow. Because this position error is so large compared to the error for the pitot-static probe, the use of a hemispherical flow-direction sensor is recommended as a backup airspeed sensor only. Additional tests to determine the best location for static ports on the cylindrical portion of the hemispherical flow-direction sensor may be of interest.

CONCLUDING REMARKS

Flow-direction data were obtained from a hemispherical flow-direction sensor which was flight tested on an F-104 airplane. The flight tests covered an angle-of-attack range of 0° to 13°, a Mach number range of 0.5 to 1.8, and an altitude range of 6.1 kilometers (20,000 feet) to 12.2 kilometers (40,000 feet). The flight data were compared with wind-tunnel data for hemispherical flow-direction sensors. The hemispherical flow-direction sensor was also compared with a NACA A-6 pitot-static probe for possible airspeed application. Analysis of the flight and wind-tunnel data showed that the calibration curves were linear for angles of attack up to 13° over the test Mach number range.

A comparison of the sensitivity parameters showed that the agreement of the flight and wind-tunnel data was fairly good at subsonic Mach numbers and improved in the transonic Mach number range. The agreement between the flight and wind-tunnel data was good at Mach numbers above 1.2.

An uncertainty in angle of attack of $\pm 0.35^{\circ}$ or less was obtained over most of the dynamic pressure range tested. Above a dynamic pressure of approximately 40 kN/m^2 (835 lb/ft^2), the uncertainty was less than $\pm 0.30^{\circ}$.

The stagnation pressures measured at the pitot-static probe tip and the center port of the hemispherical flow-direction sensor were not influenced by one another or by the supporting structure up to a Mach number of approximately 1.6. At higher Mach numbers there was some divergence between the flight and wind-tunnel data.

An airspeed position error calibration obtained by using the angle-of-attack or angle-of-sideslip ports on the hemispherical flow-direction sensor showed that the magnitude of the probe's position error increased linearly as Mach number increased. The hemispherical flow-direction sensor gave a much larger position error than the pitot-static probe.

Flight Research Center,
National Aeronautics and Space Administration,
Edwards, Calif., Sept. 7, 1973.

REFERENCES

1. Roberts, B. G.: Static Response of Hemispherical Headed, Differential Pressure Incidencemeter From M = 1.6 to 2.6. Tech. Note HSA 43, Weapons Research Establishment, Australian Defence Scientific Service, Nov. 1959.

2. Beecham, L. J.; and Collins, S. J.: Static and Dynamic Response of a Design of Differential Pressure Yawmeter at Supersonic Speeds. C.P. No. 414, British A.R.C., 1958.

3. Hutton, P. G.: Static Response of a Hemispherical-Headed Yawmeter at High Subsonic and Transonic Speeds. C.P. No. 401, British A.R.C., 1958.

4. Rogal, B.: Differential Pressure Measurements in Sensing Sideslip and Angle of Attack. Flight Test Instrumentation, Proceedings of the Third International Symposium-1964, Vol. 3, M. A. Perry, ed., Pergamon Press, 1965, pp. 1-22.

5. Mechtly, E. A.: The International System of Units - Physical Constants and Conversion Factors (Revised). NASA SP-7012, 1969.

6. Richardson, Norman R.; and Pearson, Albin O.: Wind-Tunnel Calibrations of a Combined Pitot-Static Tube, Vane-Type Flow-Direction Transmitter, and Stagnation-Temperature Element at Mach Numbers From 0.60 to 2.87. NASA TN D-122, 1959.

7. Webb, Lannie D.; and Washington, Harold P.: Flight Calibration of Compensated and Uncompensated Pitot-Static Airspeed Probes and Application of the Probes to Supersonic Cruise Vehicles. NASA TN D-6827, 1972.

8. Montoya, Earl J.: Wind-Tunnel Calibration and Requirements for In-Flight Use of Fixed Hemispherical Head Angle-of-Attack and Angle-of-Sideslip Sensors. NASA TN D-6986, 1973.

9. Larson, Terry J.; Stillwell, Wendell H.; and Armistead, Katharine H.: Static-Pressure Error Calibrations for Nose-Boom Airspeed Installations of 17 Airplanes. NACA RM H57A02, 1957.

10. Liepmann, H. W.; and Roshko, A.: Elements of Gasdynamics. Fourth ed., John Wiley & Sons, Inc., 1962.

TABLE 1.– MACH NUMBER UNCERTAINTY

Mach number	Altitude, km (ft)	Uncertainty
0.50	7.6 (25,000)	±0.015
1.00	7.6 (25,000)	±0.006
1.00	10.7 (35,000)	±0.009
1.50	7.6 (25,000)	±0.007
1.50	10.7 (35,000)	±0.007
1.80	10.7 (35,000)	±0.007
1.80	12.2 (40,000)	±0.007

TABLE 2.– ANGLE-OF-ATTACK ERROR RESULTING FROM UNCERTAINTY IN PRESSURE MEASUREMENTS

h, km (ft)	M_∞						
	0.6	0.8	1.0	1.2	1.4	1.6	1.8
	α error, deg						
7.6 (25,000)	±0.48	±0.28	±0.23	±0.18	±0.13	±0.12	±0.10
10.7 (35,000)	±0.69	±0.48	±0.35	±0.28	±0.21	±0.17	±0.13

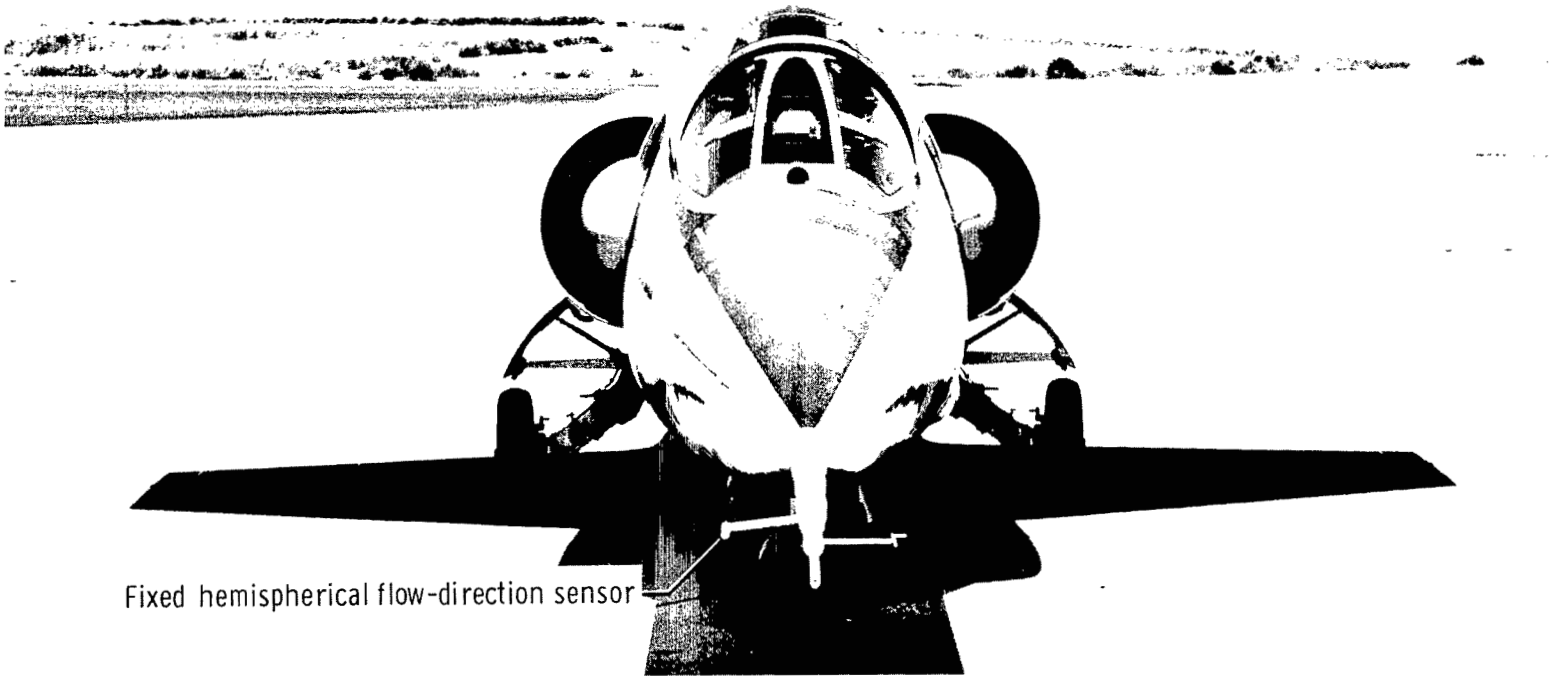

Figure 1. Photograph of F-104 airplane with fixed hemispherical flow-direction sensor installed on the nose boom.

E-20506

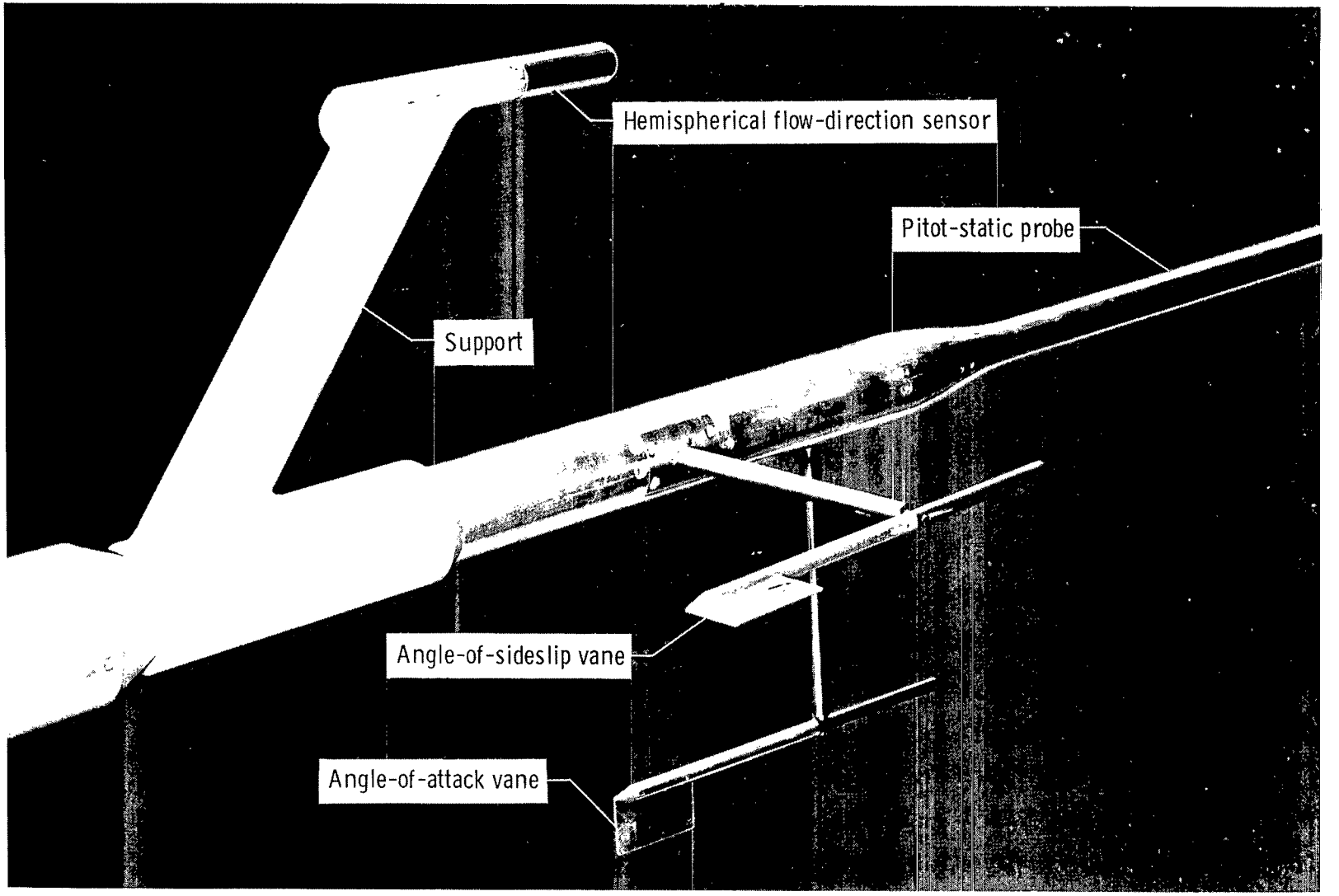

Figure 2. Hemispherical flow-direction sensor mounted on the nose boom (bottom rear view). E-21230

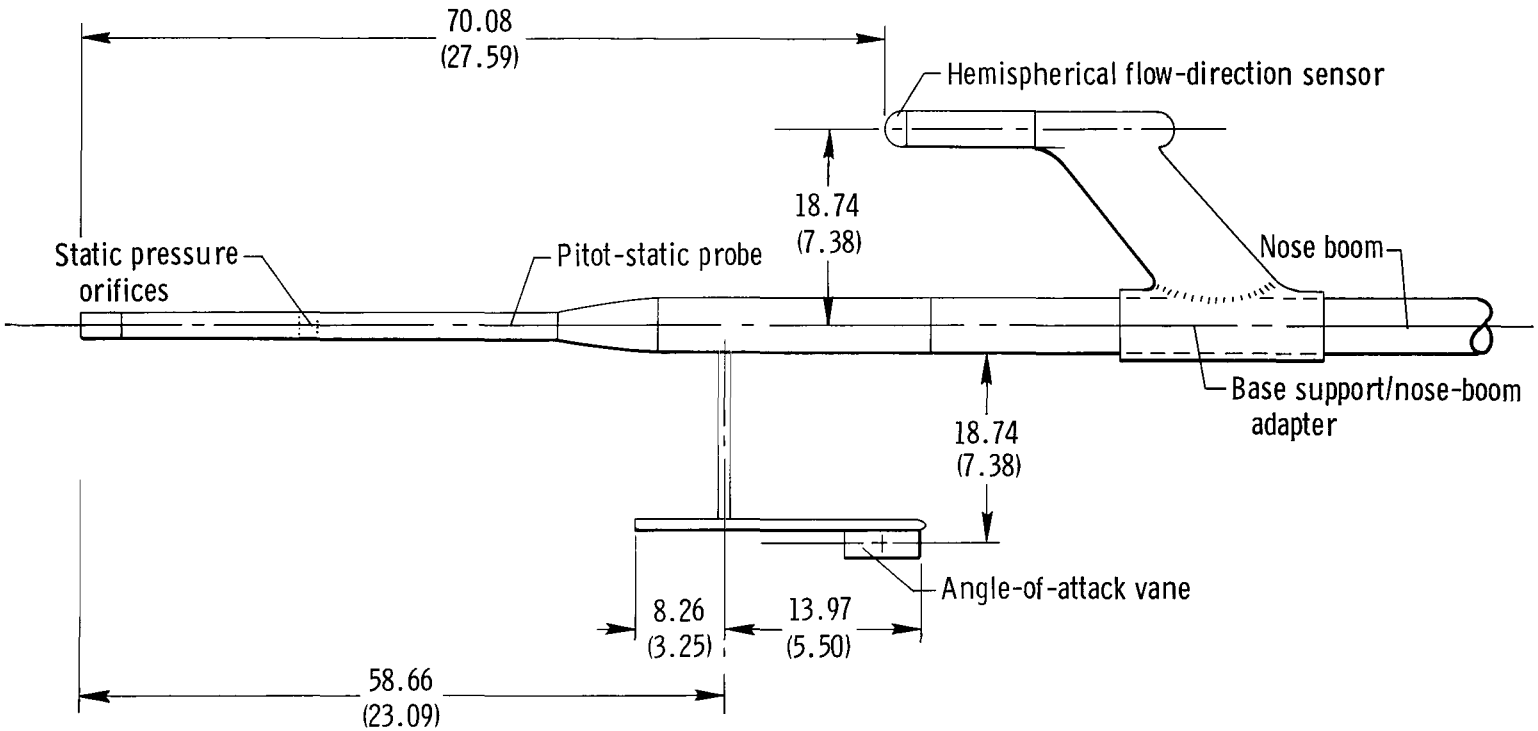

Figure 3. Diagram of the hemispherical flow-direction sensor, angle-of-attack vane, and pitot-static probe. Dimensions are in centimeters (inches).

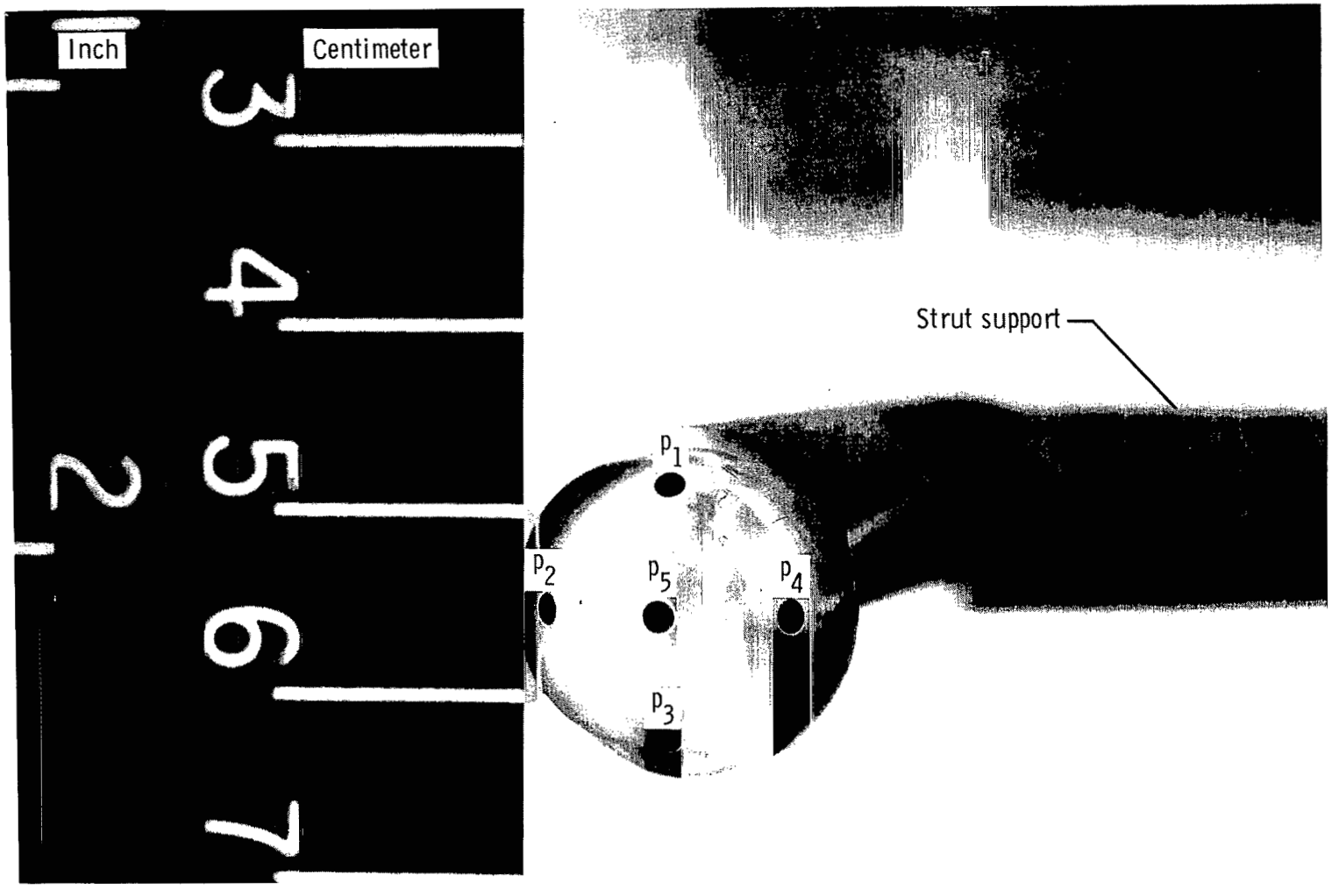

(a) Photograph of the hemispherical flow-direction sensor. E-25922

Figure 4. Hemispherical flow-direction sensor and support.

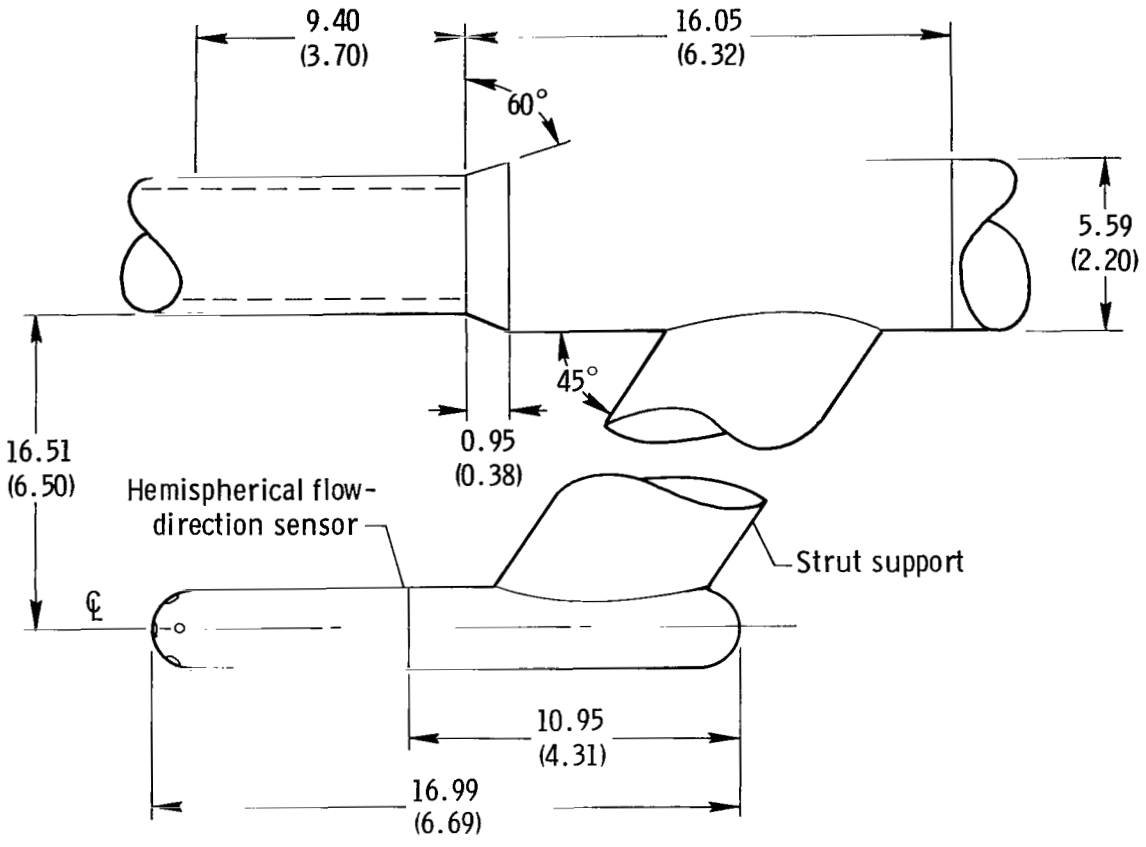

(b) Drawing of the hemispherical flow-direction sensor and support. Dimensions are in centimeters (inches) unless otherwise noted.

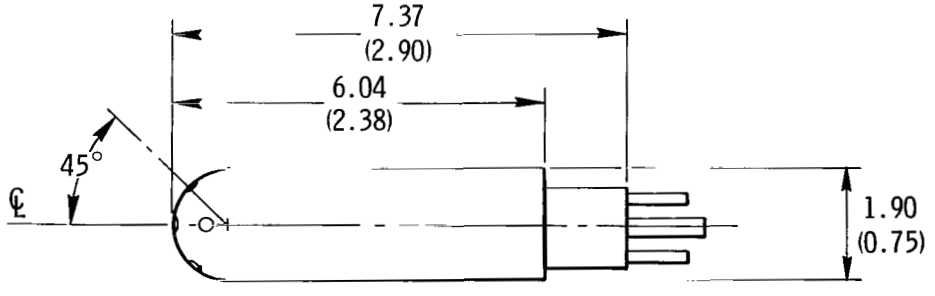

(c) Drawing of the head portion of the hemispherical flow-direction sensor. Dimensions are in centimeters (inches) unless otherwise noted.

Figure 4. Concluded.

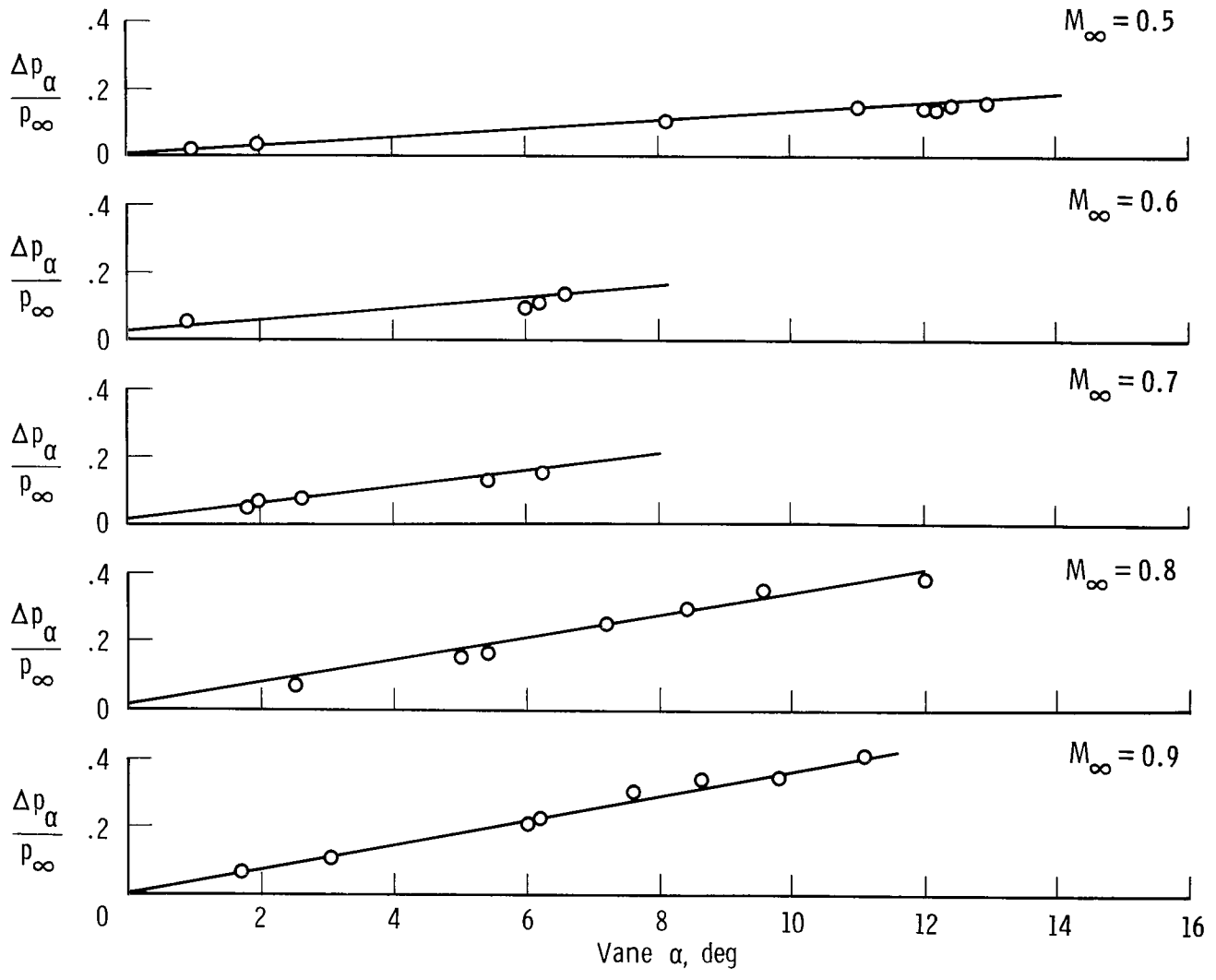

(a) M_∞ = 0.5, 0.6, 0.7, 0.8, and 0.9; h = 6.1 to 9.15 kilometers (20,000 to 30,000 feet).

Figure 5. Ratio of differential pressure between the two angle-of-attack ports to ambient pressure as a function of angle of attack for Mach numbers from 0.5 to 1.8. $\beta \approx 0^\circ$.

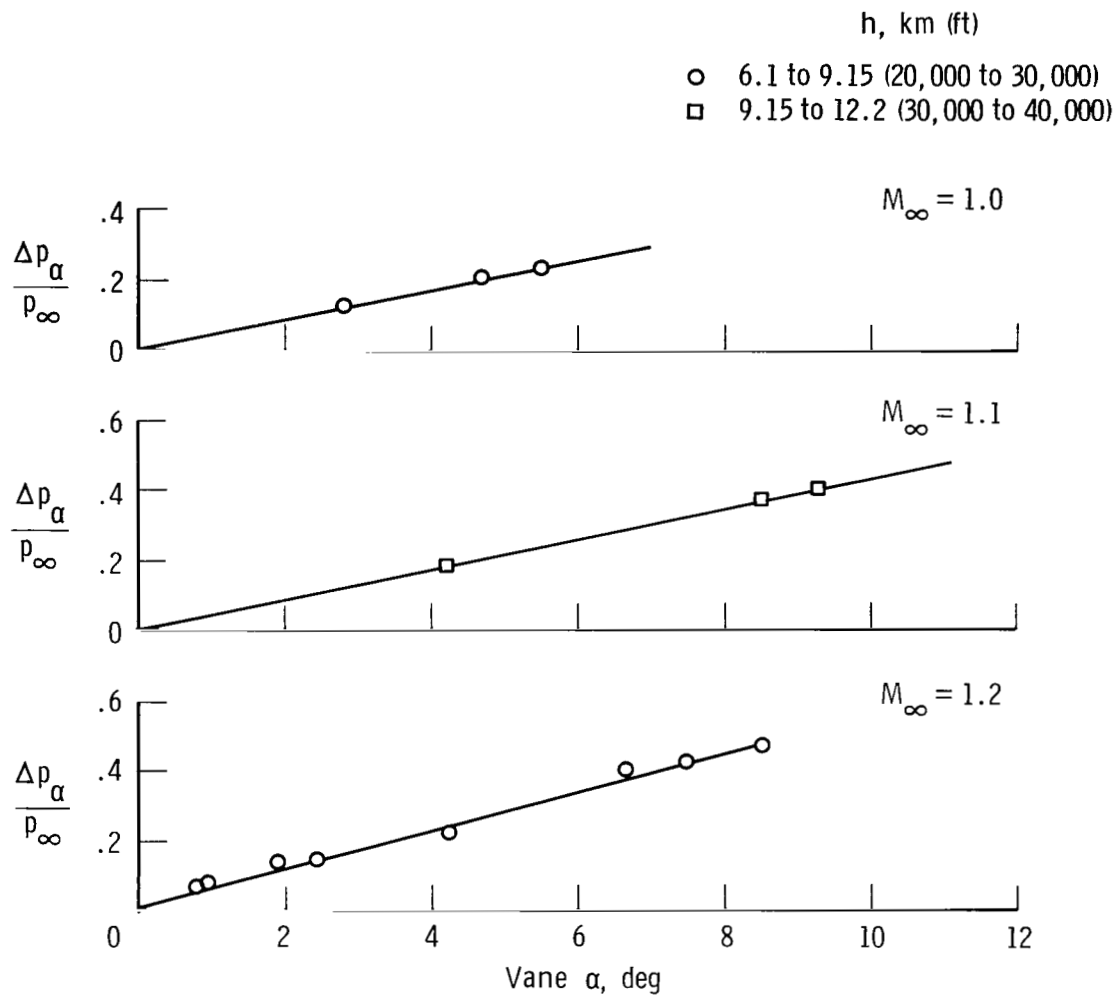

(b) $M_\infty = 1.0$, 1.1, and 1.2.

Figure 5. Continued.

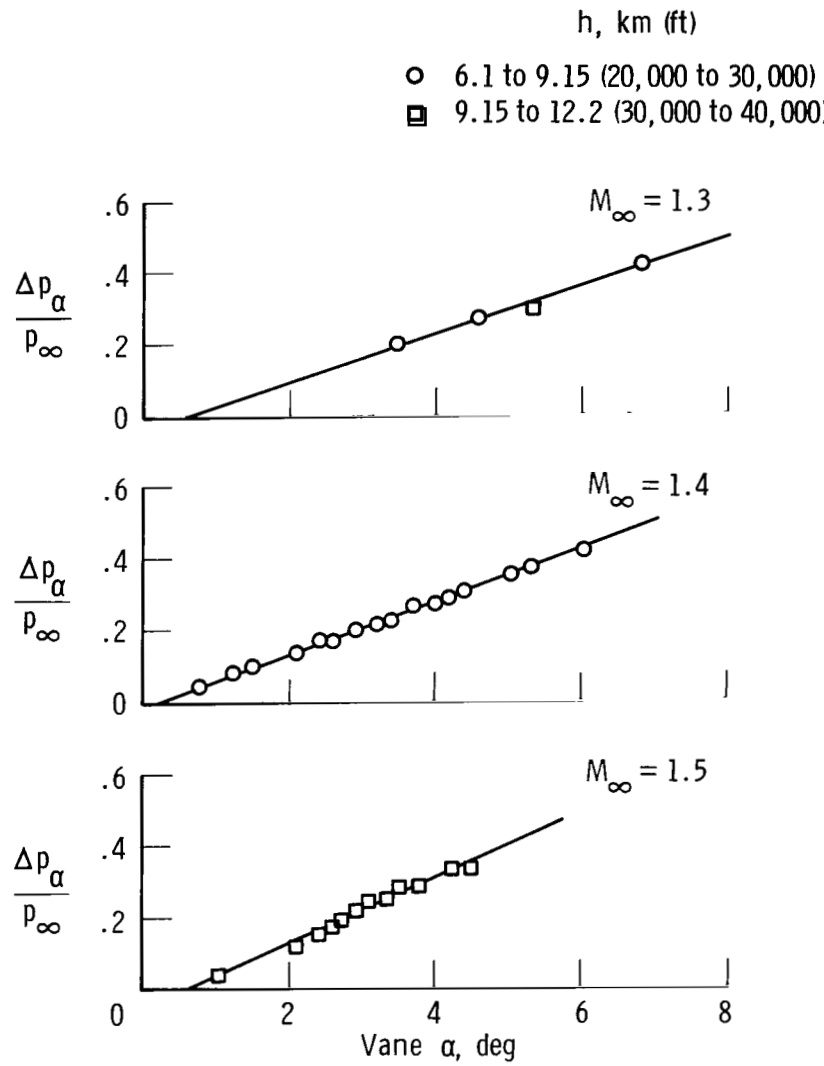

(c) $M_\infty = 1.3$, 1.4, and 1.5.

Figure 5. Continued.

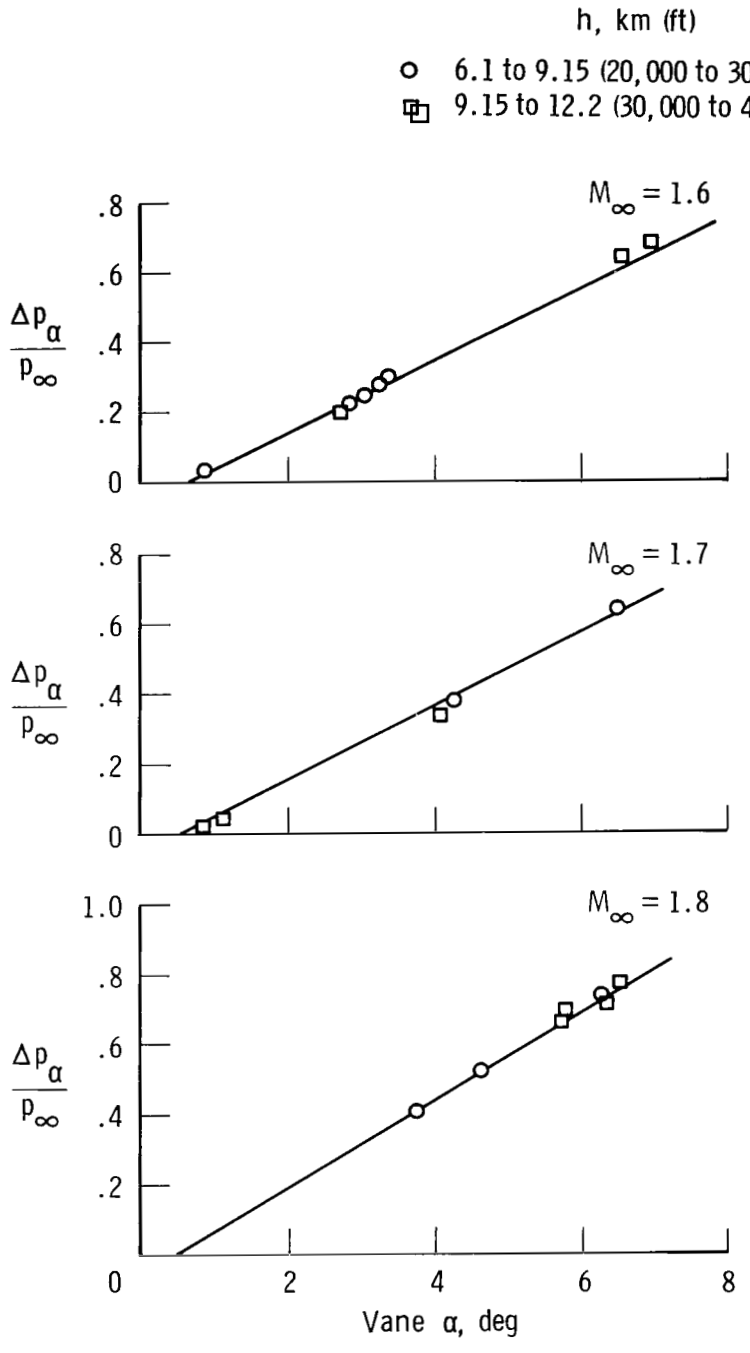

(d) $M_\infty = 1.6$, 1.7, and 1.8.

Figure 5. Concluded.

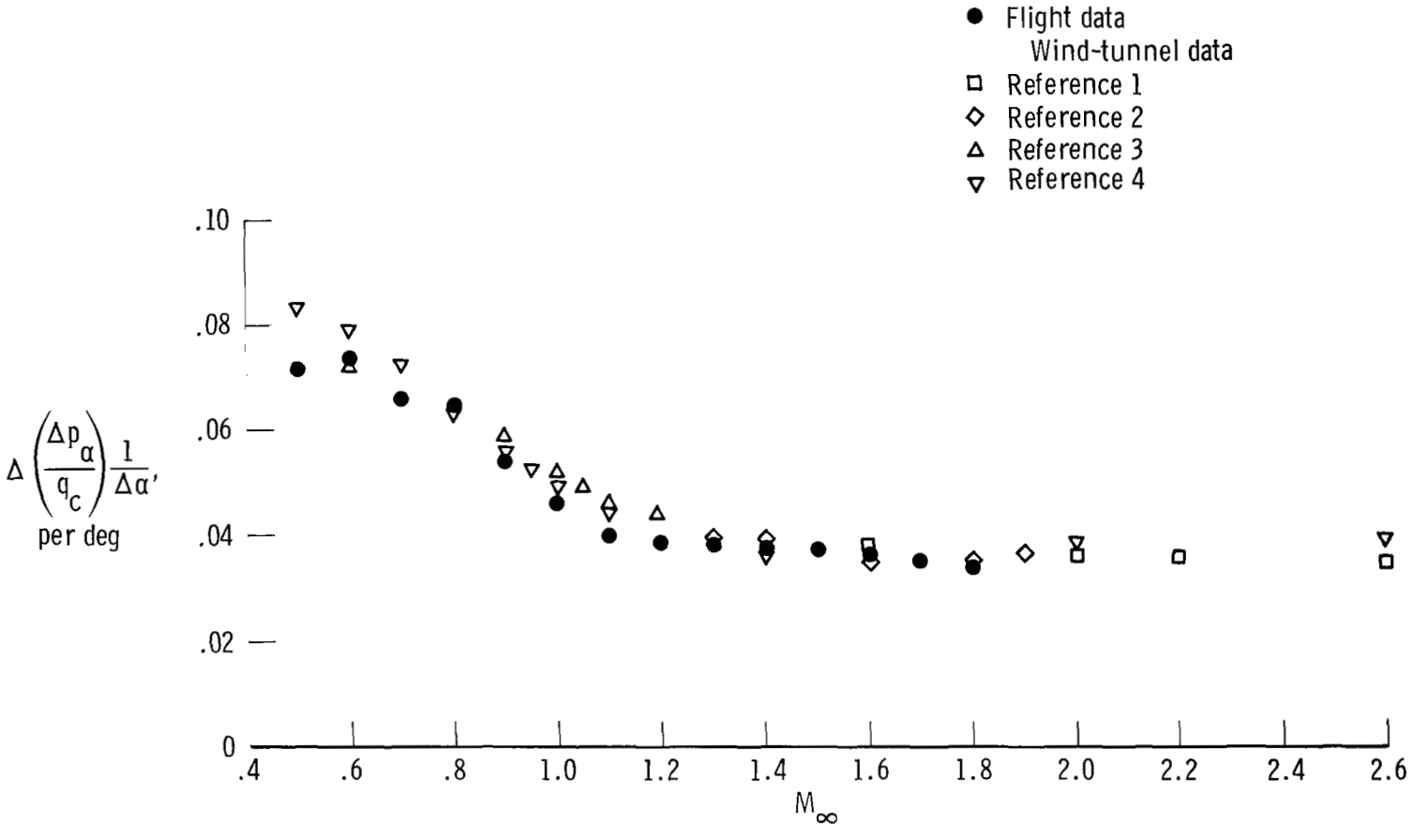

Figure 6. Comparison of wind-tunnel and flight data for the sensitivity parameter $\Delta\left(\frac{\Delta p_\alpha}{q_c}\right)\frac{1}{\Delta\alpha}$ as a function of Mach number.

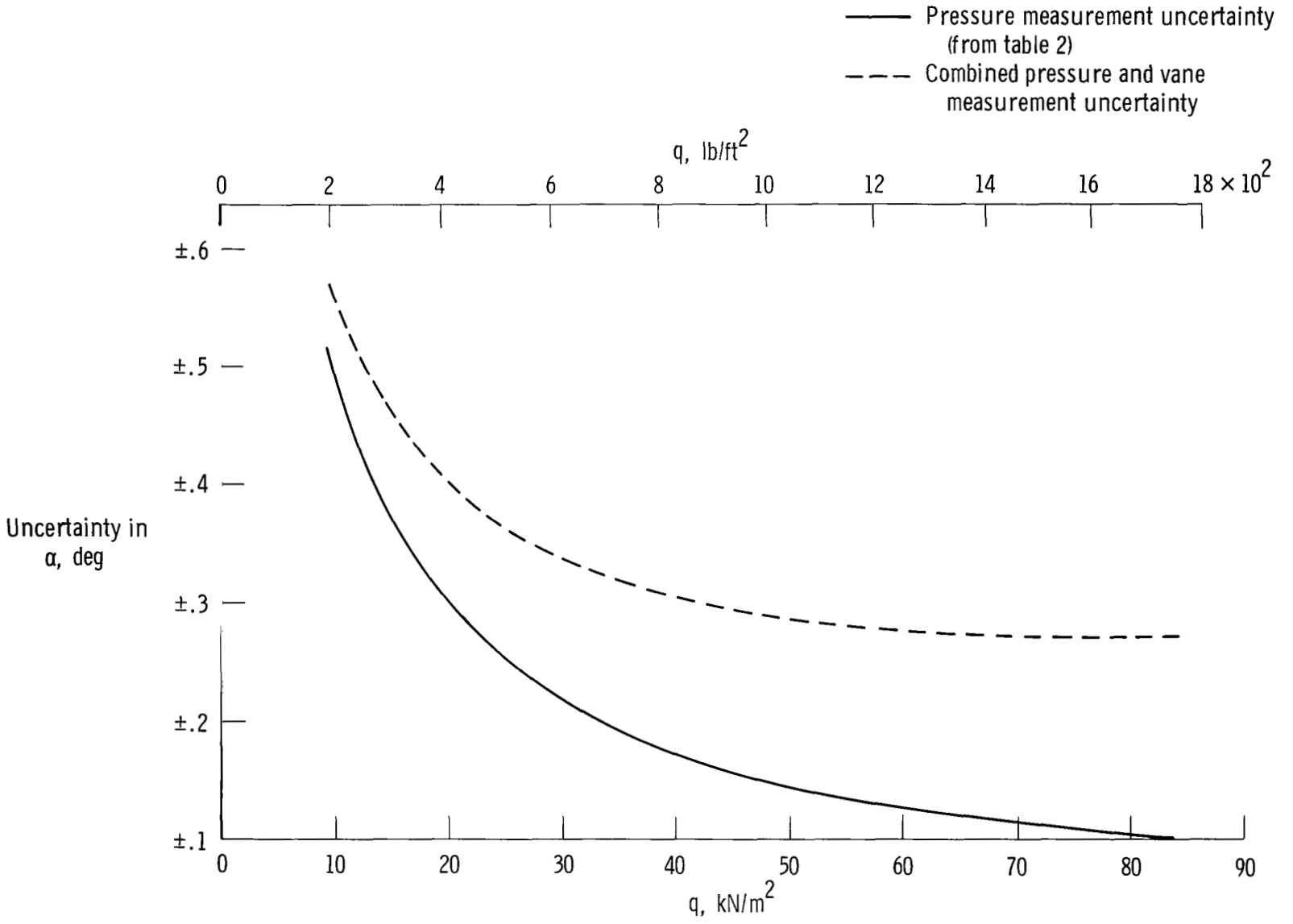

Figure 7. Calculated uncertainty in angle of attack as a function of dynamic pressure and measurement uncertainty.

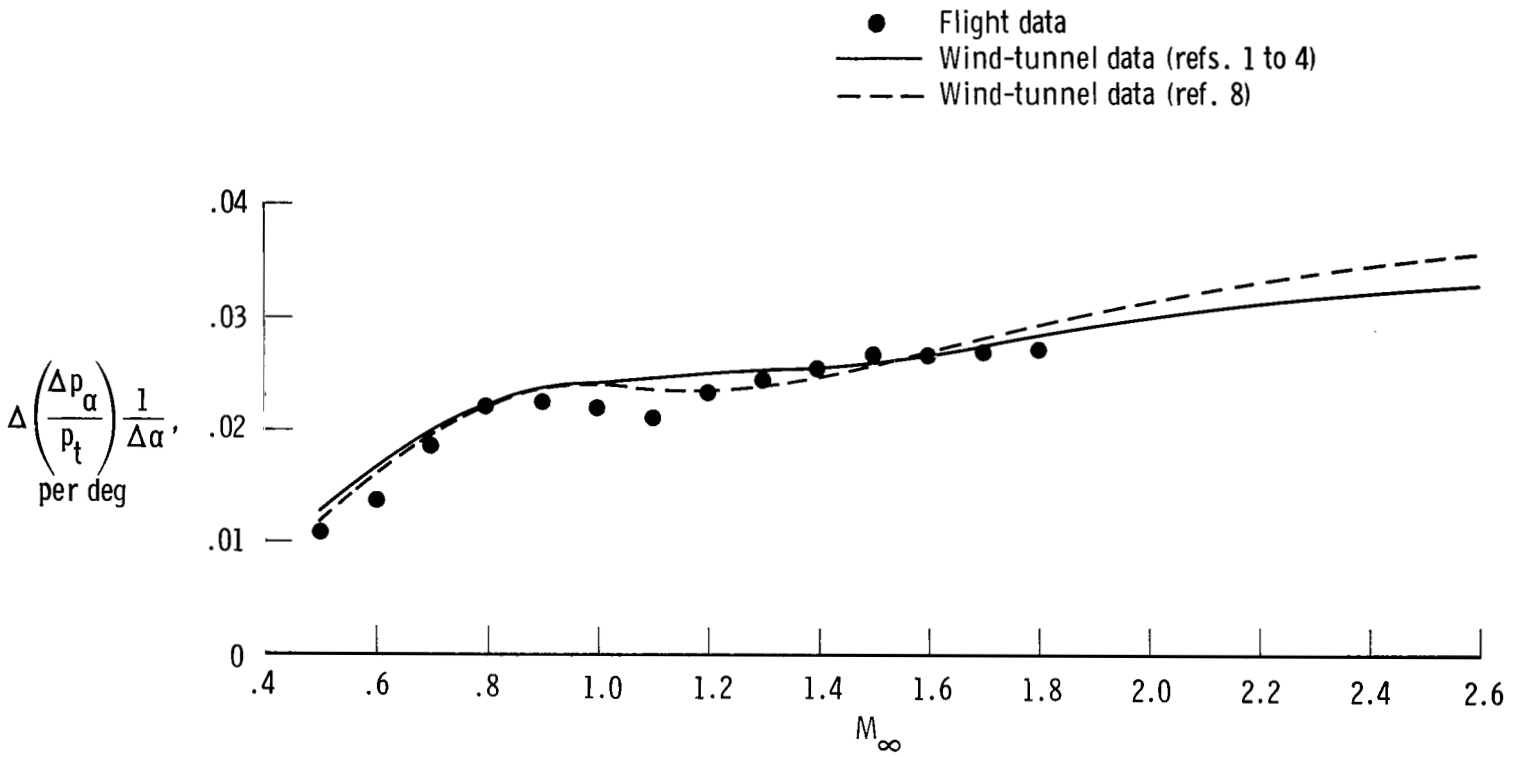

Figure 8. Comparison of wind-tunnel and flight data for the sensitivity parameter $\Delta\left(\frac{\Delta p_\alpha}{p_t}\right)\frac{1}{\Delta\alpha}$ as a function of Mach number.

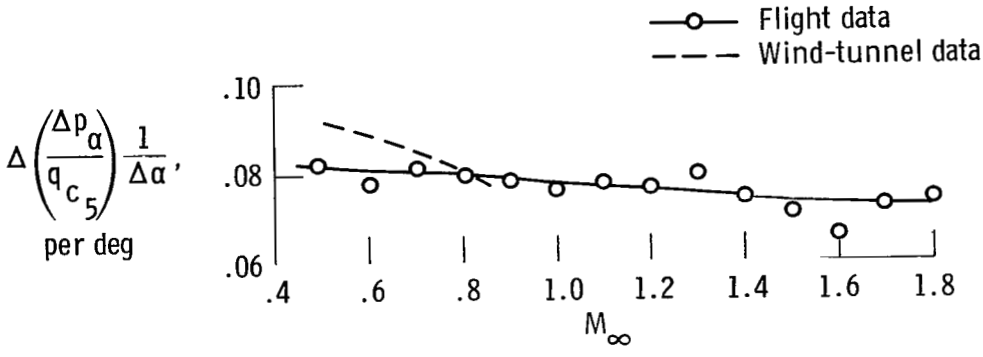

(a) Comparison of flight and wind-tunnel data for $\Delta\left(\frac{\Delta p_\alpha}{q_{c_5}}\right)\frac{1}{\Delta\alpha}$ as a function of Mach number

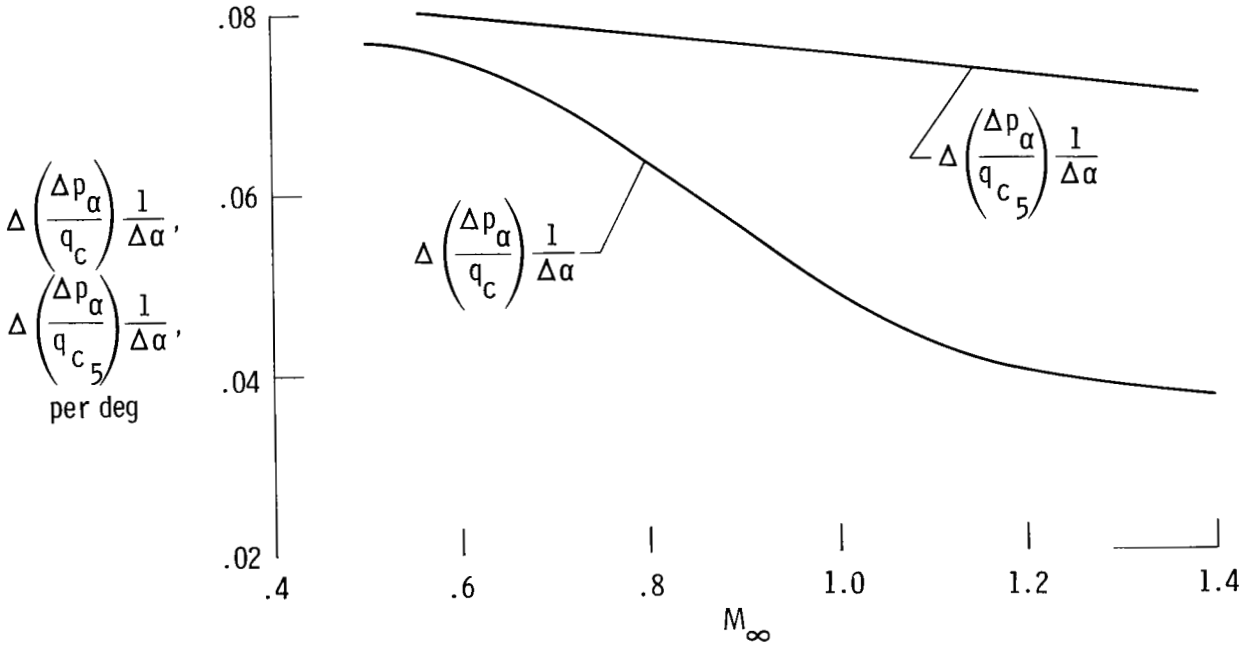

(b) Variation of $\Delta\left(\frac{\Delta p_\alpha}{q_c}\right)\frac{1}{\Delta\alpha}$ and $\Delta\left(\frac{\Delta p_\alpha}{q_{c_5}}\right)\frac{1}{\Delta\alpha}$ with Mach number.

Figure 9. Comparison of the change in sensitivity parameters $\Delta\left(\frac{\Delta p_\alpha}{q_c}\right)\frac{1}{\Delta\alpha}$ and $\Delta\left(\frac{\Delta p_\alpha}{q_{c_5}}\right)\frac{1}{\Delta\alpha}$ with Mach number.

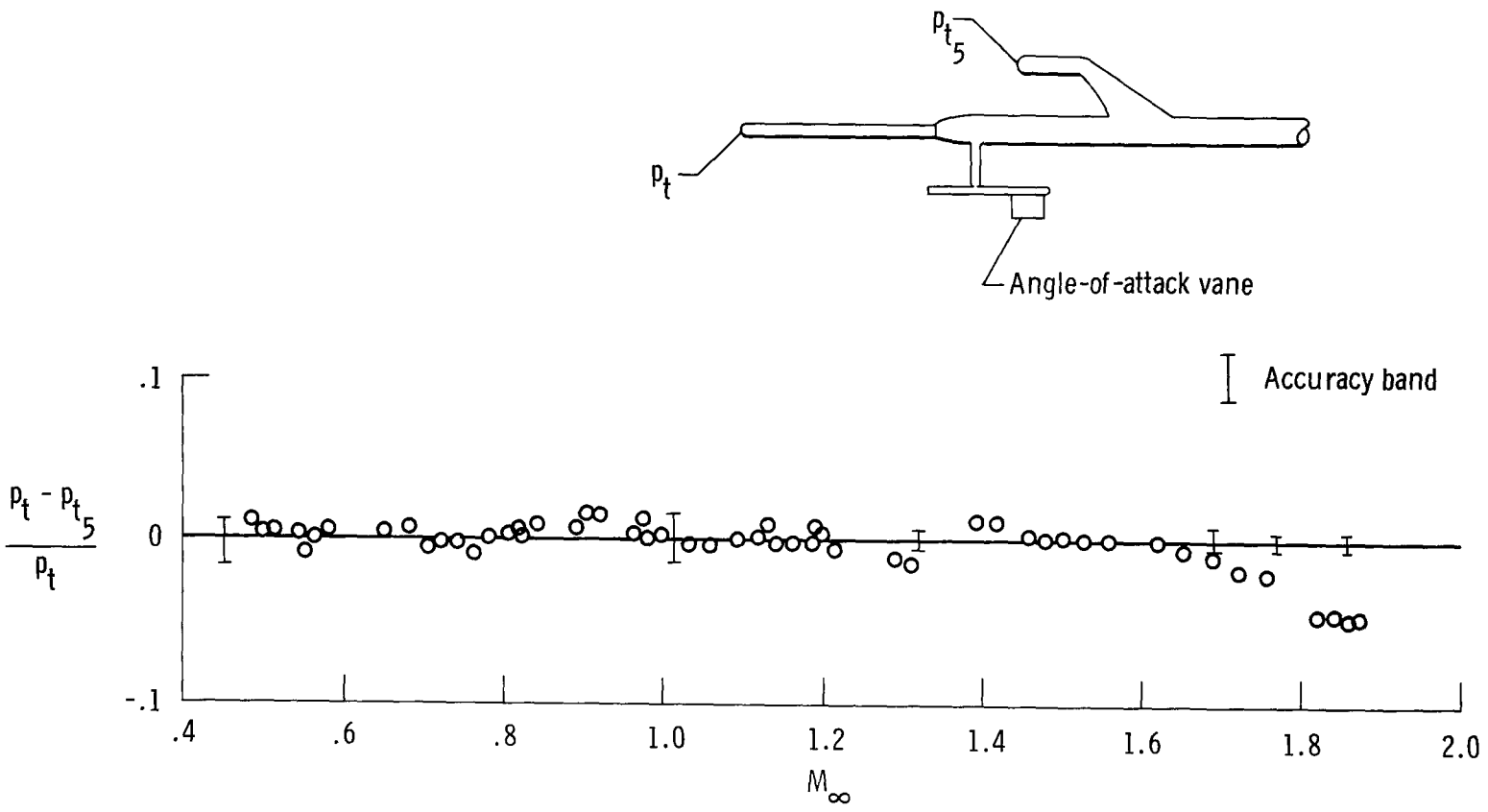

Figure 10. Comparison of stagnation pressures measured by the pitot-static probe and by the hemispherical flow-direction sensor at the p_{t_5} port. $\alpha = 0^\circ$ to 13°.

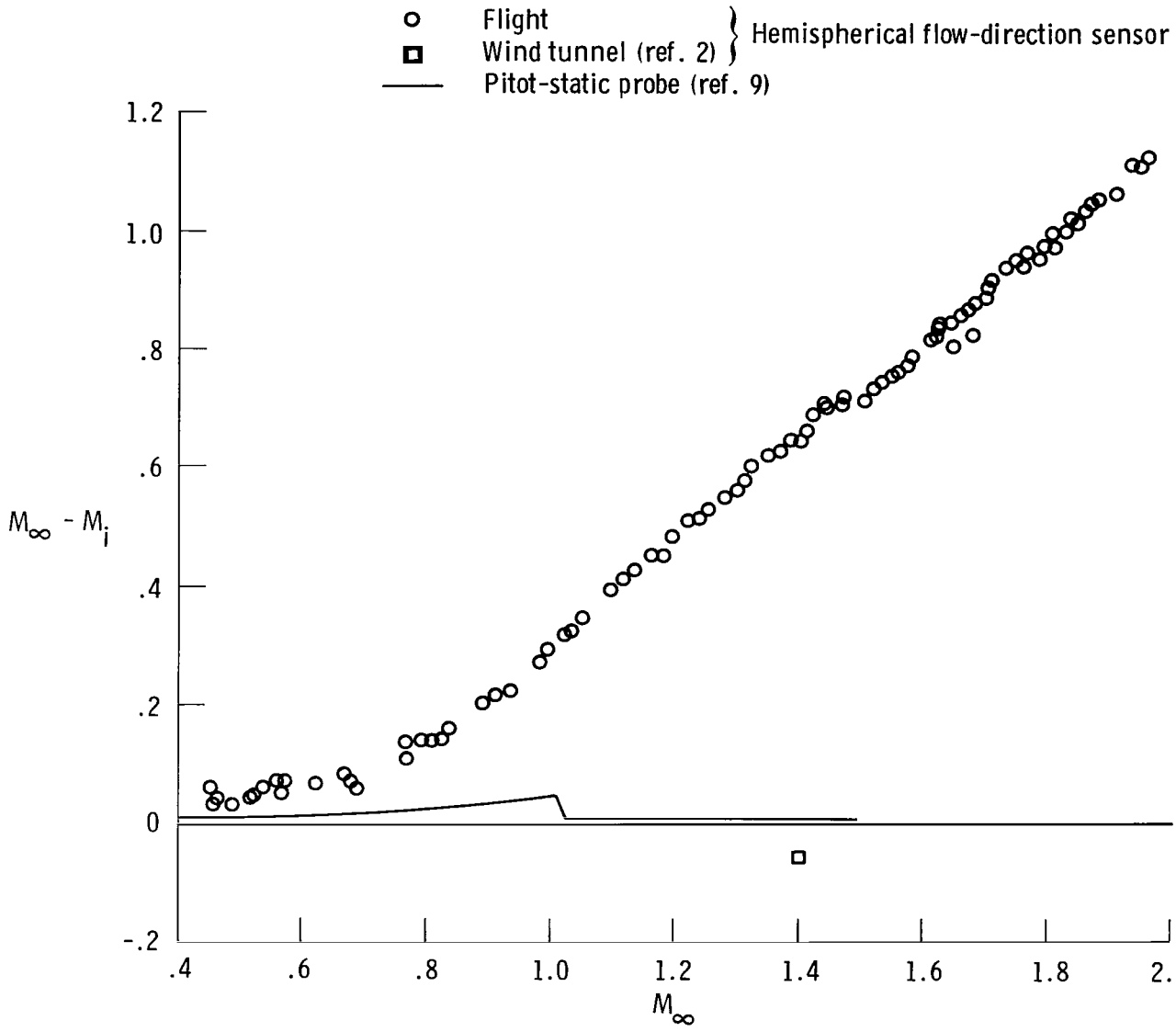

Figure 11. Comparison of Mach number position errors from the hemispherical flow-direction sensor and the pitot-static probe. $\alpha = 0^\circ$ to 13°.